Research Square

Preprints are preliminary reports that have not undergone peer review.
They should not be considered conclusive, used to inform clinical practice,
or referenced by the media as validated information.

Stratospheric Winds Shape Winter Precipitation in the American Southwest

Gregory Egger
University of Utah
Thomas Reichler
thomas.reichler@utah.edu

University of Utah

Article

Keywords:

Posted Date: August 19th, 2026

DOI: https://doi.org/10.21203/rs.3.rs-10658139/v1

License: This work is licensed under a Creative Commons Attribution 4.0 International License.
Read Full License

Additional Declarations: No competing interests reported.

Stratospheric Winds Shape Winter Precipitation in the American Southwest

Gregory Egger[1] & Thomas Reichler[1]

[1]Department of Atmospheric Sciences, University of Utah, Salt Lake City, USA

Correspondence: Thomas Reichler, thomas.reichler@utah.edu

In the dry southwestern United States, seasonal precipitation outlooks are crucial for water management. Yet these outlooks rely largely on the El Niño–Southern Oscillation (ENSO), whose influence on regional precipitation is weakest in early winter, when substantial precipitation can occur. Using observations, we show that the quasi-biennial oscillation (QBO), a regular alternation of equatorial stratospheric winds, helps narrow this gap. The QBO is most strongly associated with early-winter precipitation, whereas ENSO is more informative later. In an idealized predictability framework, adding QBO information to ENSO nearly doubles the variance explained in winter precipitation. The QBO signal is linked to a localized Pacific storm-track shift, revealing a previously unrecognized stratospheric influence on regional hydroclimate and suggesting a path toward improved outlooks for this water-limited region.

Introduction

The Southwestern United States (SWUS) is a semi-arid region whose major population centers and economic activity depend on limited water resources. Seasonal hydrological predictions can therefore support water-resource planning and management. Much of the region's annual precipitation falls in winter, when mountain snowpack stores water that sustains warm-season

streamflow[1]. Yet SWUS winter precipitation varies strongly from year to year, and seasonal totals often depend on a relatively small number of storms. Identifying large-scale circulation drivers that help anticipate this variability is central to improving SWUS hydroclimate prediction.

SWUS winter precipitation is closely tied to the North Pacific jet, whose latitude, strength, and eastward extent influence whether Pacific storm activity reaches the region. ENSO has, for decades, been the dominant source of seasonal predictability for the SWUS because it modulates this jet and the associated storm track[2,3]. However, ENSO-based predictability is uneven: the ENSO-related precipitation signal over the western U.S. strengthens from early to late winter, leaving less guidance at the start of winter[4–6]. ENSO-based predictability is also reduced during weak or neutral ENSO winters.

A promising source of additional jet-related predictability is the quasi-biennial oscillation (QBO), an alternation of equatorial stratospheric winds with a period of about 28 months[7]. Although the QBO originates in the tropical stratosphere, it has been linked to tropospheric circulation through tropical, subtropical, and high-latitude pathways[8,9]. Of particular relevance here, the QBO can modulate the North Pacific jet and storm track, providing a plausible pathway through which it may influence winter precipitation over the western U.S.[10–12]. Previous studies have used QBO information mainly for subseasonal prediction, targeting precipitation or atmospheric-river activity several weeks ahead, often in combination with the Madden–Julian Oscillation[13-15]. Whether the QBO provides predictive information on seasonal winter timescales for SWUS precipitation, how that information varies through winter, and whether it adds predictability beyond ENSO remain unresolved.

The relationship between the QBO and ENSO also matters for prediction because the two modes may not be completely independent[16,17], and their observed teleconnections can be difficult to separate[18]. This raises the question of whether QBO information improves seasonal prediction of SWUS winter precipitation beyond ENSO alone, and how that added value varies within winter.

Here, we show that the QBO provides a previously underexplored source of seasonal predictive information for SWUS winter precipitation beyond ENSO. This added signal is most apparent in early winter, when ENSO-related precipitation signals over the western U.S. are weakest, and appears to be linked to QBO-related modulation of the North Pacific jet. The following analysis quantifies the QBO influence on SWUS precipitation, evaluates its dynamical connection to the jet, and assesses how it combines with ENSO.

Results

Complementary QBO–ENSO precipitation signals

We first assess whether QBO variability is associated with precipitation over the SWUS domain during Dec–Mar, a hydrologically important period that accounts for about 41% of the region's annual precipitation. Following the lead–lag framework of Park et al.[19], we correlate the SWUS precipitation index with QBO zonal winds at individual pressure levels and with ENSO (Fig. 1). Within this core winter season, we distinguish early winter (Dec–Jan) from late winter (Feb–Mar) to capture the distinct timing of the QBO and ENSO relationships evident in monthly analyses.

Fig. 1 reveals a clear seasonal contrast. The strongest QBO relationship occurs with 70 hPa winds evaluated two months before Dec–Jan SWUS precipitation ($r = -0.55$). This

negative relationship indicates that Oct–Nov westerly QBO winds at 70 hPa are associated with anomalously dry Dec–Jan SWUS precipitation, whereas easterly QBO winds are associated with wetter anomalies. ENSO shows a different seasonal structure: its strongest correlation occurs with Feb–Mar precipitation when the ENSO index is evaluated two months after the precipitation period ($r = 0.52$), while its Dec–Jan relationship is weaker. Thus, QBO and ENSO exhibit seasonally complementary relationships with SWUS precipitation, with the QBO preferentially associated with early winter and ENSO with late winter. Some correlation maxima occur after the precipitation period and therefore indicate phase relationships, not forecast lead times; these relationships can still inform prediction because ENSO and the QBO are predictable months ahead[20,21].

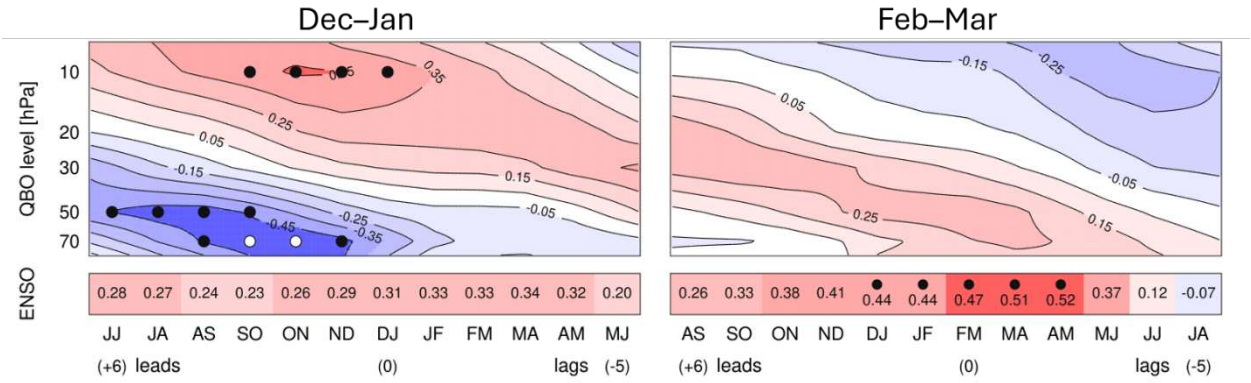


Figure 1 | SWUS precipitation correlations. Correlations between area-averaged SWUS precipitation and QBO winds at different pressure levels (top) and the ENSO index (bottom) are shown. The SWUS domain is defined as 27–42°N, 125–103°W. In this domain, Dec–Mar precipitation totals approximately 143 mm out of an annual total of 345 mm, or about 41%. The x-axis indicates predictor lead–lag month relative to the precipitation period. Black and white circles mark correlations significant at the 95% and 99% confidence levels, respectively.

We next examine the spatial structure underlying these area-averaged relationships by regressing gridded precipitation onto the selected QBO and ENSO predictors (Fig. 2), using the correlation-maximizing lead–lag offsets from Fig. 1. The resulting patterns reveal a clear seasonal separation. QBO-related precipitation anomalies are strongest in Dec–Jan, with significant negative coefficients centered over northern California and extending across the broader SWUS. ENSO-related anomalies are strongest in Feb–Mar, with significant positive coefficients over the SWUS. The QBO–Feb–Mar and ENSO–Dec–Jan patterns are weaker and less spatially extensive, indicating that the two predictors are associated with distinct seasonal precipitation signals. Correlation maps further sharpen this contrast, with strong QBO–Dec–Jan and ENSO–Feb–Mar signals but weak cross-period correlations (Supplemental Fig. 1).

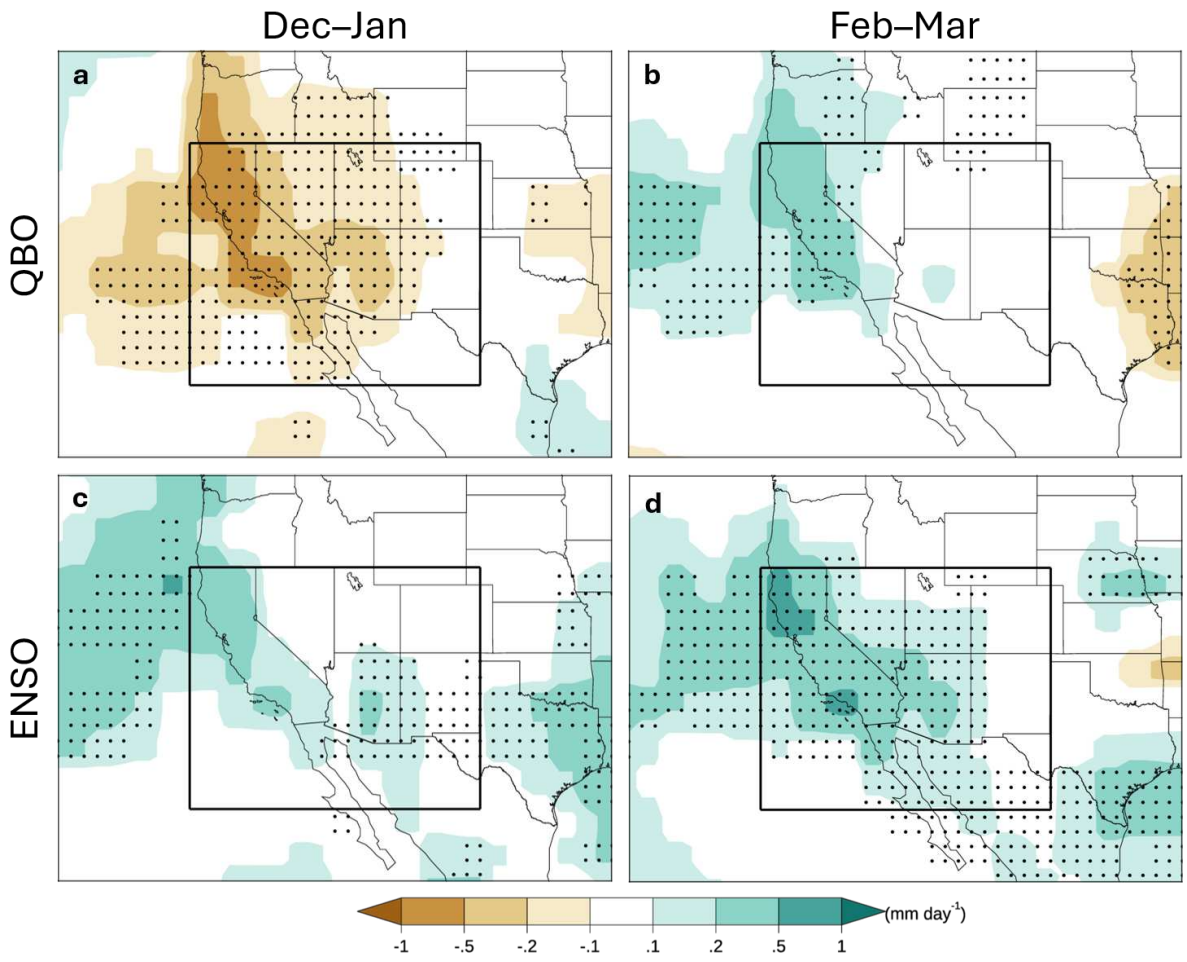


Figure 2 | Precipitation anomalies associated with QBO and ENSO. Shading shows precipitation anomalies associated with one standard deviation of the corresponding predictor. Predictors are evaluated at the correlation-maximizing lead–lag offsets identified in Fig. 1 for Dec–Jan and Feb–Mar precipitation. The box marks the SWUS averaging region used in Fig. 1 and subsequent analyses. Stippling indicates statistical significance at the 95% confidence level.

QBO-enhanced potential predictability

Next, we evaluate whether the observed QBO and ENSO relationships translate into predictive skill using a linear statistical model that predicts area-averaged SWUS precipitation from the 70 hPa QBO wind predictor and the ENSO index. The model is fit separately for Dec–Jan and Feb–

Mar, and the two predictions are then averaged to estimate Dec–Mar precipitation. The reported skill values assume that the relevant QBO and ENSO predictor values are known, so they represent a potential-predictability benchmark. This isolates the predictive information associated with the two modes before accounting for uncertainty in the predictors' forecasts.

Fig. 3 illustrates the SWUS precipitation predictability associated with the QBO and ENSO by showing the year-to-year variability of the selected predictor indices together with observed and statistically predicted Dec–Mar precipitation. Colored dots in the predictor time series mark years in which the absolute predictor anomaly exceeds 0.5 standard deviations. Because ENSO and QBO anomalies are not always both large or aligned in their implied precipitation response, only a subset of years produces a strong combined signal. These aligned-predictor years, in which both predictors exceed the threshold and imply precipitation anomalies of the same sign, are marked by check marks and crosses below Fig. 3b. In 12 of the 15 such years, the observed Dec–Mar precipitation anomaly has the predicted sign, corresponding to an 80% success rate.

The statistical prediction captures a substantial fraction of the observed Dec–Mar precipitation variability, with a cross-validated correlation of $r = 0.61$ between predicted and observed SWUS precipitation (Fig. 3c,d). The model also predicts the sign of the precipitation anomaly in 33 of 46 winters, corresponding to a 72% sign accuracy. Notably, all 13 sign errors occur for relatively modest predicted anomalies, none exceeding about one standard deviation in magnitude.

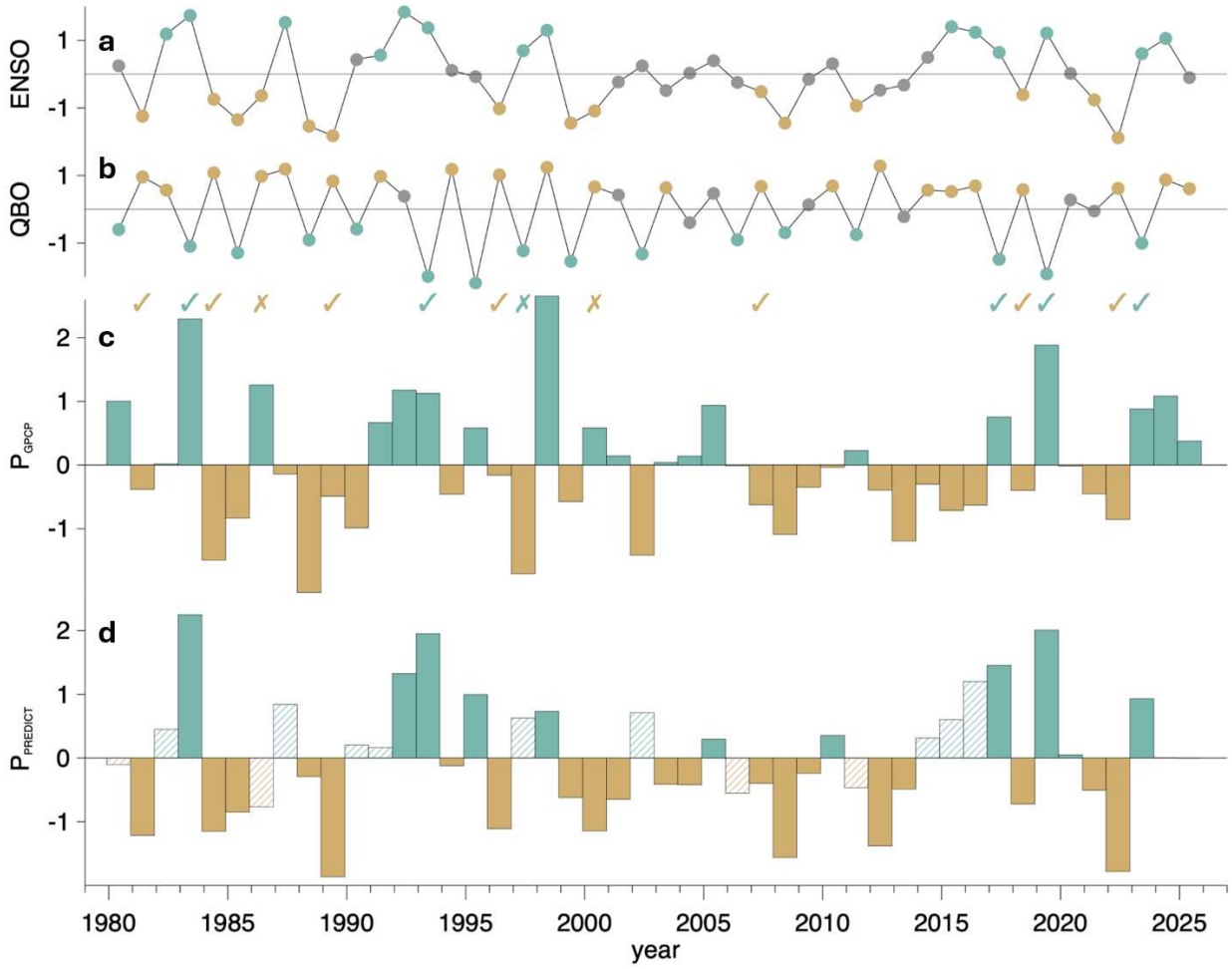


Figure 3 | Statistical prediction of SWUS Dec–Mar precipitation. Standardized anomalies are shown for winters 1979/80–2024/25 for **a**, the selected ENSO predictor, averaged over Apr–May; **b**, the 70 hPa QBO wind predictor, averaged over Oct–Nov; **c**, observed GPCP Dec–Mar SWUS precipitation; and **d**, statistically predicted Dec–Mar SWUS precipitation. The cross-validated correlation between observed and predicted precipitation is $r = 0.61$. Colored dots in **a** and **b** mark predictor anomalies exceeding ± 0.5 standard deviations; color indicates the sign of the observed Dec–Mar precipitation anomaly. Crosses and check marks below **b** indicate failed and successful sign predictions, respectively, for years in which both predictors exceed ± 0.5 standard deviations and their regression-implied precipitation anomalies have the same sign; 80% of these cases are successful. Hatched bars in **d** mark years when predicted and

observed precipitation anomalies have opposite signs; overall, predicted and observed signs agree in 72% of years.

The variance explained by the full and single-predictor models is summarized in Supplemental Fig. 2. For Dec–Mar, the combined prediction explains 37% of the variance in SWUS precipitation, compared with 21% for the ENSO-only benchmark. Thus, incorporating QBO information via separate Dec–Jan and Feb–Mar predictions improves skill over the ENSO-only benchmark.

By contrast, a QBO-only model fit directly to Dec–Mar precipitation explains only 4% of the variance, consistent with the opposite signs of the QBO–precipitation relationship in early and late winter (Fig. 2). The period-specific models clarify this behavior. In Dec–Jan, the QBO-only model explains substantially more variance than the ENSO-only model, whereas in Feb–Mar the opposite is true (Supplemental Fig. 2). The QBO therefore provides most of the early-winter predictive skill, while ENSO dominates in late winter, consistent with Figs. 1 and 2. In both periods, the combined QBO–ENSO model explains more variance than either single-predictor benchmark, indicating that the two modes provide complementary predictive information.

QBO-related jet and storm-track displacement

Because the QBO influence on SWUS precipitation is strongest in Dec–Jan, we focus on this period to investigate the associated circulation anomalies. We regress zonal wind and eddy kinetic energy (EKE) onto the Oct–Nov 70hPa QBO wind predictor (Fig. 4). The QBO-related 250 hPa zonal wind response forms a meridional dipole over the North Pacific and western North America, with strengthened westerlies to the north and weakened westerlies to the south, consistent with a poleward displacement of the upper-tropospheric flow. This is the only

159 extratropical feature in the zonal wind field that remains significant at the 99% confidence level
160 (not shown).

161 The 250 hPa EKE response, used here as a storm-track diagnostic, shows a similar
162 meridional dipole, spanning roughly 150–90°W, with enhanced EKE poleward of the
163 climatological storm-track region and reduced EKE to the south[22]. This indicates a poleward
164 shift in transient eddy activity accompanying the QBO-related Dec–Jan zonal wind response.
165 Together, these responses suggest that the QBO-related Dec–Jan signal reflects a broader
166 reorganization of the upper-tropospheric jet and storm-track structure rather than a local wind
167 anomaly near the coast.

168 The ENSO-related zonal wind and EKE anomalies during Feb–Mar also form a
169 meridional dipole (Supplemental Figs. 3 and 4), but it is centered farther south than the
170 corresponding QBO–Dec–Jan pattern. By contrast, the QBO–Feb–Mar and ENSO–Dec–Jan
171 anomalies are weak and mostly not statistically significant over the SWUS, consistent with the
172 weaker precipitation signals in Figs. 1 and 2.

173 Returning to the QBO-related Dec–Jan response, the meridional cross sections in Fig.
174 4c,d examine the vertical structure of the zonal-wind and EKE dipoles identified above. Over the
175 135–105°W longitude band, the QBO-related Dec–Jan zonal wind anomalies bear some
176 resemblance to the well-known horseshoe-shaped pattern[10]. Across the SWUS latitude range, the
177 zonal wind anomalies form a statistically significant meridional dipole within the broader
178 westerly flow, while the EKE anomalies show a corresponding poleward displacement of
179 transient eddy activity relative to the climatological storm track. Together, these cross sections
180 indicate that, in this sector, both the mean westerly flow and transient eddy activity are displaced
181 poleward through much of the troposphere. The ENSO-related Feb–Mar zonal-wind cross

section is stronger and opposite-signed, but primarily reinforces the climatological jet structure rather than producing a comparable meridional dipole (Supplemental Fig. 5). The EKE cross sections show dipole-like anomalies for all predictor–period pairings, but statistically significant anomalies in both lobes are clearest for QBO–Dec–Jan and ENSO–Feb–Mar (Supplemental Fig. 6).

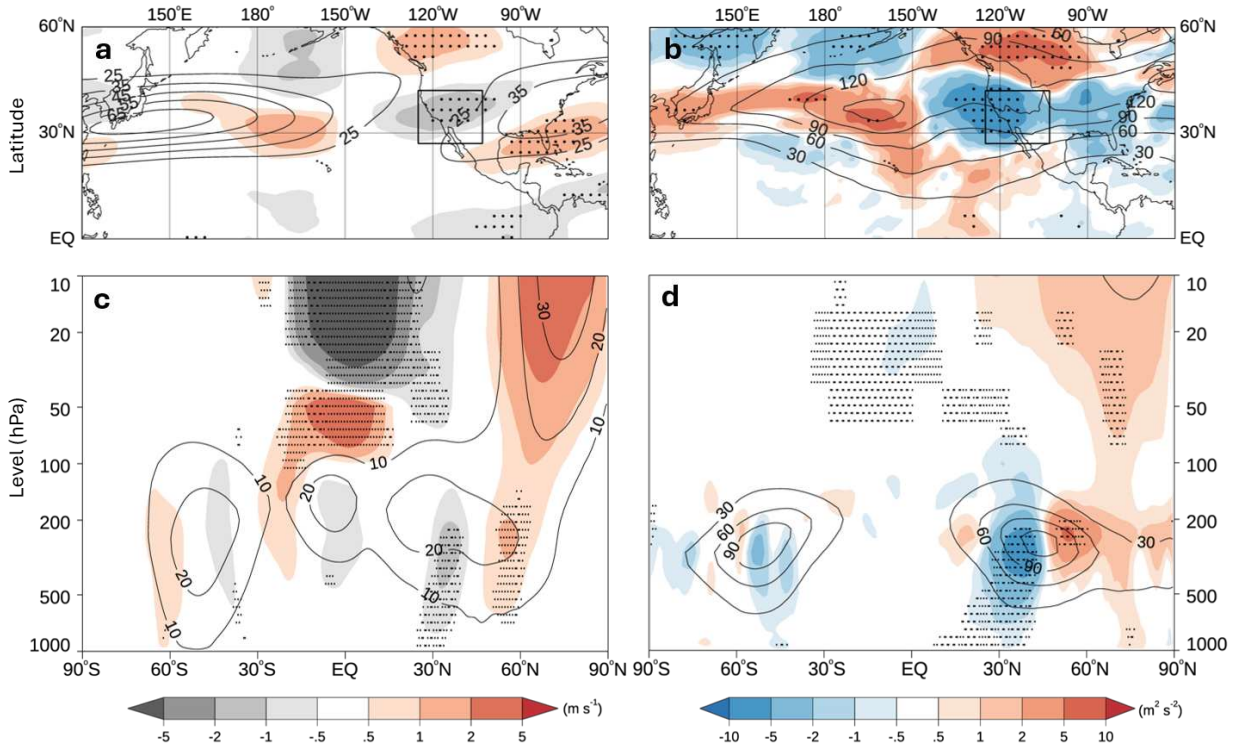


Figure 4 | QBO-related jet and eddy-activity anomalies. Shading shows Dec–Jan anomalies associated with one standard deviation of the Oct–Nov 70-hPa QBO wind predictor for **a**, 250 hPa zonal wind; **b**, 250 hPa eddy kinetic energy (EKE); **c**, zonal wind averaged over 135–105°W; and **d**, EKE averaged over 135–105°W. Black contours show the corresponding climatologies. The box in **a** and **b** marks the SWUS region. Stippling indicates statistical significance at the 95% confidence level.

Discussion

This study identifies the QBO as a previously underexplored source of seasonal predictive information for SWUS winter precipitation beyond ENSO. The QBO contributes most strongly to prediction during early winter, when the ENSO influence is relatively weak, whereas ENSO provides stronger information later in winter. This seasonal separation explains why combining the two modes improves Dec–Mar precipitation prediction relative to an ENSO-only benchmark. In an idealized potential-predictability framework, the combined model reaches a cross-validated $r = 0.61$, near the ~ 0.6 benchmark for useful forecast skill[23], while explaining substantially more SWUS precipitation variance than ENSO alone. The associated circulation response provides a dynamical basis for this improvement: the QBO is linked to a poleward shift of upper-tropospheric westerlies and transient eddy activity over western North America during early winter.

The QBO-related Dec–Jan circulation response may also involve the stratospheric polar vortex. In the QBO phase associated with reduced Dec–Jan SWUS precipitation, the tropical lower stratosphere is characterized by westerly equatorial winds near 70 hPa (Fig. 4). Correspondingly, Arctic stratospheric winds are also anomalously westerly, consistent with the Holton–Tan relationship[24]. These westerly Arctic anomalies extend downward and equatorward, suggesting that polar-vortex variability may contribute to the poleward branch of the tropospheric wind dipole over western North America. Similar downward-extending zonal mean wind anomalies have been documented during weak and strong polar-vortex events[25,26]. However, those studies examine event-centered, zonal-mean vortex composites rather than the regional Dec–Jan QBO response identified here.

This distinction raises the possibility that the early-winter Holton–Tan pathway has a regionally structured tropospheric expression over western North America. The robustness of the QBO-related western North American zonal-wind dipole is consistent with this view: it is the only extratropical feature in the zonal-wind field that remains significant at the 99% confidence level. Recent analysis further shows that the observed Holton–Tan relationship strengthens in early winter, peaks in January, weakens in February, and reverses sign in March[27]. The QBO–SWUS precipitation relationship identified here shows a similar seasonal evolution, with a strong Dec–Jan signal and a much weaker, opposite-signed Feb–Mar response (Fig. 2a,b). This parallel seasonality is consistent with a polar-vortex contribution to the early-winter QBO signal, but the potential overlap between the QBO's polar and subtropical pathways makes their relative contributions difficult to isolate from observations[8,28]. Targeted modeling experiments are therefore needed to distinguish these mechanisms.

An immediate application of these results is to extend ENSO-based SWUS winter outlooks with QBO information. The winter 2026/27 outlook provides a timely example. El Niño conditions are expected to strengthen into that season (Climate Prediction Center, ENSO Diagnostic Discussion, 11 June 2026; accessed 10 August 2026), while the regular progression of the QBO suggests easterly 70 hPa conditions following the westerly lower-stratospheric phase during much of 2025 (NASA Goddard Space Flight Center, QBO monitoring page; accessed 10 August 2026). If realized, this combination would tilt the odds toward anomalously wet SWUS conditions, with the easterly QBO favoring early-winter precipitation and El Niño favoring later-winter precipitation. The coming winter, therefore, provides a real-time opportunity to evaluate whether the complementary QBO and ENSO influences identified here translate into actionable seasonal guidance.

Methods

Data sources and preprocessing

We use monthly precipitation from the Global Precipitation Climatology Project (GPCP)[29]. Atmospheric fields are taken from the ECMWF ERA5 reanalysis[30], which is used to analyze atmospheric circulation and to construct the QBO and ENSO indices. Monthly zonal-wind fields are used for the mean-flow analysis, while daily winds are used to compute transient eddy kinetic energy (EKE). All datasets span 1979–2025 (46 winters) and are analyzed on a 1° × 1° grid. Unless otherwise noted, all variables are expressed as anomalies relative to the climatological mean for each calendar month and are linearly detrended before analysis.

Predictor indices and storm-track diagnostics

The QBO is represented by zonal-mean equatorial (5°S–5°N) zonal winds at individual stratospheric pressure levels. Lead–lag relationships with SWUS precipitation are evaluated separately for each level using two-month-mean QBO indices. The 70-hPa QBO index is used because it exhibits the strongest relationship with Dec–Jan SWUS precipitation. ENSO is represented by the Niño-3.4 sea-surface temperature index, derived from ERA5 skin temperature. Both predictor indices are averaged over the corresponding two-month predictor windows.

Following Blackmon[31], transient eddy kinetic energy (EKE) is derived from zonal and meridional winds after applying a 2–8-day band-pass filter to isolate synoptic-scale eddies associated with midlatitude storm tracks. EKE is defined as $\mathrm{EKE} = \frac{1}{2}[(u')^2 + (v')^2]$, where u' and v' denote the band-pass-filtered zonal and meridional wind anomalies, respectively. The

resulting EKE fields are averaged over the corresponding monthly or two-month analysis periods.

Statistical analysis

Correlations and regression coefficients between seasonal anomalies and the QBO and ENSO predictors are computed for all variables shown. Statistical significance is assessed using two-tailed Student's *t* tests[32]. Because the QBO is a persistent quasi-periodic oscillation rather than a simple AR(1) process, we use conservative effective degrees of freedom of $\nu = n/2$ for QBO-related tests, whereas the nominal value of $\nu = n - 2$ is used for ENSO-related tests. Unless stated otherwise, statistical significance refers to the 95% confidence level.

Statistical model

We use multiple linear regression to predict SWUS precipitation from the QBO (Q) and ENSO (E) indices. Separate regression models are constructed for Dec–Jan and Feb–Mar precipitation using the optimal predictor windows identified in Fig. 1:

$$P'_{DJ} = a_{DJ} + b_{DJ}Q_{ON} + c_{DJ}E_{MA},$$

$$P'_{FM} = a_{FM} + b_{FM}Q_{MA} + c_{FM}E_{AM},$$

where P'_{DJ} and P'_{FM} denote SWUS precipitation anomalies during Dec–Jan and Feb–Mar, respectively. The subscripts indicate the two-month averaging periods of the predictor indices (ON = Oct–Nov, MA = Mar–Apr, and AM = Apr–May). The Dec–Mar prediction is obtained by averaging the predicted Dec–Jan and Feb–Mar anomalies: $P'_{DJFM} = \frac{1}{2}\left(P'_{DJ} + P'_{FM}\right)$. For comparison, additional regression models are constructed using either ENSO or the QBO alone for Dec–Jan, Feb–Mar, and Dec–Mar precipitation. These provide benchmark models for evaluating the combined QBO–ENSO prediction.

Model validation

Statistical models are validated using repeated 5-fold cross-validation. For each realization, the 46 winters are randomly partitioned into five groups. Four groups are used to train the model, and the remaining group serves as the validation set. This procedure is repeated until each group has served once as the validation set, and the entire cross-validation is repeated 100 times using different random partitions to reduce sensitivity to the specific data split. Model skill is quantified by the mean cross-validated correlation between observed and predicted SWUS precipitation, computed by averaging Fisher z-transformed correlations and then transforming the result back to correlation space[33]. Explained variance is reported as $R^2 = r^2$, where r is the mean cross-validated correlation.

References

1. Barnett, T. P., Adam, J. C. & Lettenmaier, D. P. Potential impacts of a warming climate on water availability in snow-dominated regions. *Nature* **438**, 303–309 (2005).
2. Trenberth, K. E. et al. Progress during TOGA in understanding and modeling global teleconnections associated with tropical sea surface temperatures. *J. Geophys. Res. Oceans* **103**, 14291–14324 (1998).
3. Cayan, D. R., Redmond, K. T. & Riddle, L. G. ENSO and hydrologic extremes in the western United States. *J. Clim.* **12**, 2881–2893 (1999).
4. Jong, B. T. et al. El Niño's impact on California precipitation: Seasonality, regionality, and El Niño intensity. *Environ. Res. Lett.* **11**, 054021 (2016).
5. Gershunov, A. & Barnett, T. P. Interdecadal Modulation of ENSO Teleconnections. *Bull. Amer. Meteor. Soc*., **79**, 2715–2726 (1998).
6. Peings, Y., Dong, C. & Magnusdottir, G. Seasonality in the predictive skill of Southwest United States precipitation in the seasonal forecast systems. *Geophys. Res. Lett.* **52**, e2025GL115972 (2025).
7. Baldwin, M. P. et al. The quasi-biennial oscillation. Rev. Geophys. 39, 179–229 (2001).
8. Gray, L. J. et al. Surface impacts of the quasi-biennial oscillation. *Atmos. Chem. Phys.* **18**, 8227–8247 (2018).
9. Anstey, J. A et al. Impacts, processes and projections of the quasi-biennial oscillation. *Nat. Rev. Earth Environ*. **3**, 588–603 (2022).
10. Garfinkel, C. I. & Hartmann, D. L. The influence of the quasi-biennial oscillation on the troposphere in winter in a hierarchy of models. Part I: Simplified dry GCMs. *J. Atmos. Sci.* **68**, 1273–1289 (2011).

11. Garfinkel, C. I. & Hartmann, D. L. The influence of the quasi-biennial oscillation on the troposphere in winter in a hierarchy of models. Part II: Perpetual winter WACCM runs. *J. Atmos. Sci.* **68**, 2026–2041 (2011).
12. Wang, J., Kim, H.-M. & Chang, E. K. M. Interannual modulation of Northern Hemisphere winter storm tracks by the QBO. *Geophys. Res. Lett.* **45**, 2786–2794 (2018).
13. Mundhenk, B. D. et al. Skillful empirical subseasonal prediction of landfalling atmospheric river activity using the Madden–Julian oscillation and quasi-biennial oscillation. *npj Clim. Atmos. Sci*. **1**, 20177 (2018).
14. Nardi, K. M. et al. Skillful all-season S2S prediction of U.S. precipitation using the MJO and QBO. *Weather Forecast.* **35**, 2179–2198 (2020).
15. Castellano, C. M. et al. Development of a statistical subseasonal forecast tool to predict California atmospheric rivers and precipitation based on MJO and QBO activity. *J. Geophys. Res. Atmos.* **128**, e2022JD037360 (2023).
16. Serva, F., Cagnazzo, C., Christiansen, B. & Yang, S. The influence of ENSO events on the stratospheric QBO in a multi-model ensemble. *Clim. Dyn*. **54**, 2561–2575 (2020).
17. Rodrigo, M., García-Serrano, J. & Bladé, I. Quasi-Biennial oscillation influence on tropical convection and El Niño variability. *Geophysical Research Letters*, **52**, e2024GL112854 (2025).
18. Naoe, H. et al. QBOi El Niño–Southern Oscillation experiments: teleconnections of the QBO, *Weather Clim. Dynam.*, **6**, 1419–1442 (2025).
19. Park, C.-H., Son, S.-W., Lim, Y. & Choi, J. Quasi-biennial oscillation-related surface air temperature change over the western North Pacific in late winter. *Int. J. Climatol*. **42**, 4351–4359 (2022).

20. Barnston, A. G. et al. Skill of real-time seasonal ENSO model predictions during 2002–11: Is our capability increasing? *Bull. Am. Meteorol. Soc.* **93**, 631–651 (2012).
21. Scaife, A. A. et al. Predictability of the quasi-biennial oscillation and its Northern Hemisphere winter teleconnection on seasonal to decadal timescales. *Geophys. Res. Lett.* **41**, 1752–1758 (2014).
22. Blackmon, M. L., Wallace, J. M., Lau, N.-C. & Mullen, S. L. An observational study of the Northern Hemisphere wintertime circulation. *J. Atmos. Sci.* **34**, 1040–1053 (1977).
23. Krishnamurti, T. N. et al. Improved skill for the anomaly correlation of geopotential heights at 500 hPa. *Mon. Weather Rev.* **131**, 1082–1102 (2003).
24. Holton, J. R. & Tan, H.-C. The influence of the equatorial quasi-biennial oscillation on the global circulation at 50 mb. *J. Atmos. Sci.* **37**, 2200–2208 (1980).
25. Limpasuvan, V., Thompson, D. W. J. & Hartmann, D. L. The life cycle of the Northern Hemisphere sudden stratospheric warmings. *J. Clim.* **17**, 2584–2596 (2004).
26. Limpasuvan, V., Hartmann, D. L., Thompson, D. W. J., Jeev, K. & Yung, Y. L. Stratosphere–troposphere evolution during polar vortex intensification. *J. Geophys. Res. Atmos.* **110**, D24101 (2005).
27. Andrews, M. B. et al. Extratropical teleconnections in a multi-model ensemble nudged towards the observed QBO. Preprint at https://doi.org/10.5194/egusphere-2026-737 (2026).
28. Rao, J., Garfinkel, C. I. & White, I. P. How does the quasi-biennial oscillation affect the boreal winter tropospheric circulation in CMIP5/6? *J. Clim.* **33**, 8975–8996 (2020).
29. Adler, R. F. et al. The Version 2 Global Precipitation Climatology Project (GPCP) monthly precipitation analysis (1979–present). *J. Hydrometeorol.* **4**, 1147–1167 (2003).

30. Hersbach, H. et al. The ERA5 global reanalysis. *Q. J. R. Meteorol. Soc.* **146**, 1999–2049 (2020).
31. Blackmon, M. L. A climatological spectral study of the 500 mb geopotential height of the Northern Hemisphere. *J. Atmos. Sci.* **33**, 1607–1623 (1976).
32. von Storch, H. & Zwiers, F. W. *Statistical Analysis in Climate Research* (Cambridge Univ. Press, Cambridge, 1999).
33. Wilks, D. S. *Statistical Methods in the Atmospheric Sciences*, 4th edn (Elsevier, Amsterdam, 2020).

Author contributions

T.R. conceptualized the study. G.E. carried out the primary analysis, with contributions from T.R. G.E. drafted the initial manuscript, and both authors contributed to the final version. All authors read and approved the final manuscript.

Acknowledgements

We acknowledge the Center for High Performance Computing at the University of Utah for computational resources and support. We also thank ECMWF, the Copernicus Climate Change Service, and the GPCP for making the reanalysis and precipitation datasets publicly available. This work was supported by the U.S. Air Force Institute of Technology (G.E.) and by the National Science Foundation under grant no. 2439958 (T.R.). The funders played no role in study design, data collection, analysis and interpretation of data, or the writing of this manuscript.

Competing interests

All authors declare no financial or non-financial competing interests.

Additional information

Correspondence and requests for materials should be addressed to Thomas Reichler.

Data availability

All datasets used in this study are publicly available. Monthly precipitation data from the Global Precipitation Climatology Project are available from the NOAA National Centers for Environmental Information, https://doi.org/10.7289/V56971M6. ERA5 monthly pressure-level

and single-level reanalysis data are available from the Copernicus Climate Data Store, https://doi.org/10.24381/cds.6860a573 and https://doi.org/10.24381/cds.f17050d7. ERA5 hourly pressure-level data used to compute eddy kinetic energy are available from the Copernicus Climate Data Store, https://doi.org/10.24381/cds.bd0915c6. The derived indices and processed data used to generate the figures are available from the corresponding author upon reasonable request.

Code availability

The underlying code for this study is not publicly available but may be made available to qualified researchers on reasonable request from the corresponding author.

Supplementary Files

This is a list of supplementary files associated with this preprint. Click to download.

- Supplementalfigures.pdf